

Section C

Effects of Magnetic Fields on Highly Energetic Processes and Emission from Astrophysical Plasmas

Interaction of Gravitationally Contracting Gas Having Angular Momentum with Magnetic Field, and the Acceleration and Collimation of Astrophysical Jets

Y. Uchida, M. Nakamura, T. Miyagoshi, T. Kobayashi, T. Mukawa, and
S. Hirose

*Physics Department, Science University of Tokyo, Shinjuku-ku, Tokyo
162-8601, Japan*

Abstract. In the present paper, we stress the importance of the magnetic field in the problem of acceleration and collimation of astrophysical jets, and discuss our proposed generic picture for such “central gravitator + jets + lobes” systems and inherent interpretations of the various observational characteristics of such systems: Mechanisms are proposed for (1) the enhanced liberation of gravitational energy at the central object, (2) the transfer of a part of the liberated energy along the large-scale magnetic field by large-amplitude, torsional Alfvén wave trains that form collimated jets (we call this a sweeping pinch process), (3) the dumping of the transferred energy at the end of the jets when they impinge on the denser region outside the border of the “cavity” from which the mass contracted to the central condensation (central gravitator + accretion disk, as well as the larger-scale condensation surrounding them), and (4) the formation of wiggled jets and lobes as helical kinks and the tucked-up magnetic field produced in the sweeping pinch process, respectively.

1. Introduction

Radio jets and lobes associated with active galactic nuclei (AGN) have been known from the early days of radio astronomy. The mechanism for their production, however, has not been clarified yet. What is very clear is that they are seen in synchrotron emission in which a magnetic field of considerable strength plays an essential role together with high-energy electrons, and there is a possibility that the dynamics of the jets and lobes may also be affected, or rather, controlled, by the magnetic field.

1.1. Magnetic Field Observations

The accumulating radio polarization data in recent years, especially the advanced observations of the Faraday Rotation-corrected distributions of the projected magnetic field vectors, together with the distribution of the Faraday Rotation Measure (FRM) itself, will give us essential information about the magnetic field configuration in jets and tails. The FRM is basically due to the foreground media, but it can also be due to the contribution from the outer shell of the jets (or tails) themselves if the high-energy electrons are preferentially injected in

the core part of the jets (or tails) and the magnetic field in the outer shell serves as a Faraday rotator. This is likely to be the case, especially when there are features in the distribution of FRM having a scale as small as the width of the jets (or tails) because, otherwise, we must assume that thin layers of oppositely signed magnetic field lie side by side in the foreground intergalactic medium, exactly along our line-of-sight to the thin jet structure.

As for the straight part of the jets, the observed orderedness of the projected magnetic vectors in a certain appreciable number of the jets, with all the effects disordering such features in the observation, may be taken to indicate that this is an intrinsic feature. Namely, the direction of the projected magnetic vectors are systematically tilted from the direction of jet axis, and the FRM has opposite signs on both sides of the jet (if we subtract the FRM values that are slowly varying along the axis as foreground effect, e.g., NGC 6251: Perley, Bridle, & Willis 1984). Those two things suggest that the magnetic field in the jet may be helical. M87 may be another example showing a similar situation (Perlman et al. 1999; Owen, Hardee, & Cornwell 1989), among a number of others.

Another feature related to this is that the structural wiggles of the jet have an interesting correlation with the projected magnetic field vectors and the distribution of FRM. The recent observation of FRM in 3C449 by Feretti et al. (1999) suggests that the largest contribution to it seems to come from the magnetic field *associated* with the jets and tails themselves (Figure 2 of Uchida 2000, these Proceedings—much clearer in the original color figure) because the distribution of the sign of FRM symmetrically varies with the distance from the core and changes sign *in relation with* the bending of the jets and tails. This suggests that the greatest contribution to the FRM must come from the surface layers of the jets and tails themselves. The distribution of FRM and the projected field in the observed jets and tails of 3C465 obtained by Eilek & Owen (2000) are also very systematically correlated with the wiggling of the structure, just like the threads in the thick, wiggled rope in front of a Shinto shrine. This also seems to be difficult to attribute to the large-scale distribution of nB_{\parallel} in the foreground.

If these recent results of advanced, magnetic field measurements indicate that the magnetic field inside the jets and tails has a systematic structure, and the wiggles are structural helices in 3D, a very important restriction can be made on the models as will be described in the following. (See additional arguments by Uchida 2000, these Proceedings.)

1.2. Models Proposed Thus-far

In the early phase of research, many gas-dynamic models were given, probably because of the term “jets”. It is clear by now, however, that such models unfortunately left out the essential ingredient—the magnetic field. Here, we consider models in the context of the observed magnetic field.

Models considering the magnetic field may be divided into three categories. One is to explain the jet as a magnetically channelled flow in which the condition for a steady flow to be able to pass through the three MHD critical points is pursued. The magnetic field has a role of giving appropriate channelling without playing any other active roles. The second one, corresponding to the magnetic, centrifugal wind model of stellar winds, assumes magnetic field lines with fixed

location of the footpoints and fixed angles to the surface of the accretion disk (Blandford & Payne 1982; Pudritz & Norman 1986). The gas in the surface layer of the disk is considered to be centrifugally accelerated and goes up along the field in the rotation (up to the Alfvén point). The third one, by Uchida & Shibata (1985), made a step forward from those and actually dealt with the problem in a more realistic manner by numerical simulation using the fast computers which started developing in those days. They solved an MHD equation system with the interplay of a gravitationally contracting mass having angular momentum with a magnetic field. Uchida et al. (1999) have treated the full magnetohydrodynamic problem in 3D.

2. Magnetodynamic Model for Astrophysical Jets

Our model was first applied to the star-formation jet case (Uchida & Shibata 1985). Since the central condensation takes place from a small part of a giant molecular cloud which is highly filamentary (nothing other than the presence of magnetic field can explain such a filamentary state), we assumed that the system in which the star is formed has a large-scale, weak magnetic field in the primordial state.

The angular-momentum component of the gas perpendicular to the field may have been damped through the generation of Alfvén waves which escaped along the field, and, therefore, the angular-momentum component remaining in the later development of the system tends to be preferentially parallel to the initial, large-scale field. This means that the axis of the accretion disk that is to be formed in the later phase tends to be parallel to the initial, large-scale field.

As the mass inside the sphere contracts gravitationally, the weak field frozen-in to the gas is bunched and intensified to a considerable strength in the central part, affecting the process occurring there. The magnetic field, now having a considerable strength (but still passive), is pulled around the axis by the heavy gas disk rotating with a near-Keplerian velocity, and the toroidal component of the field is created continuously. This, as the reaction, exerts braking on the rotation of the disk material by magnetic tension, and the disk material that is braked, losing its centrifugal force, can gradually fall towards the central object, releasing the gravitational energy.

On the other hand, the magnetic field in the large “cavity” from which the mass contracted to the central region is likely to have the shape of an hourglass with the accretion disk rotating at the very narrow throat of it. In this process, the part of the magnetic field extending out of the disk is also pulled to the azimuthal direction around the axis. This causes large-amplitude, torsional Alfvén wave trains (TAWT) that propagate in both directions along the axis, bringing the unwound distant part of the hourglass-shaped field progressively into twist. The hourglass-shaped field is made into a slender structure due to the magnetic pinching progressing along the axial directions. In this process of dynamic pinching, the gas, both in the halo of the disk and in the part along the path of the propagation, is *driven* into a jet spinning helically in the same direction as the rotation of the accretion disk in our sweeping pinch model, as seen in Figure 1b. The wiggled structure frequently observed in the shape of jets may be attributed to the helical kink instability of the jet shape by the accu-

mulation of magnetic twist (Figure 2), rather than due to the Kelvin-Helmholtz instability, which has been shown to be very effectively stabilized in the presence of large-scale magnetic field in our calculation.

2.1. Equation System, and Initial and Boundary Conditions

The system of nondimensionalized equations to describe this is:

$$\frac{\partial v_r}{\partial t} + (\mathbf{v} \cdot \nabla v_r) = -\frac{C_1}{\rho} \frac{\partial p}{\partial r} + \frac{C_2}{4\pi\rho} \left[B_z \frac{\partial B_r}{\partial z} - \frac{\partial}{\partial r} (B_r^2 + B_z^2) \right] - C_3 g_r + \frac{v_\phi^2}{r}, \tag{1}$$

$$\frac{\partial v_z}{\partial t} + (\mathbf{v} \cdot \nabla v_z) = -\frac{C_1}{\rho} \frac{\partial p}{\partial z} + \frac{C_2}{4\pi\rho} \left[B_r \frac{\partial B_z}{\partial r} - \frac{\partial}{\partial z} (B_r^2 + B_z^2) \right] - C_3 g_z, \tag{2}$$

$$\frac{\partial}{\partial t} (r^2 \Omega) + r \mathbf{v} \cdot \nabla (r \Omega) = \frac{2}{4\pi\rho} \mathbf{B}_p \cdot \nabla B_\phi, \tag{3}$$

$$\frac{\partial (rA)}{\partial t} + \mathbf{v} \cdot \nabla (rA) = 0, \tag{4}$$

$$\frac{\partial B_\phi}{\partial t} + r \mathbf{v} \cdot \nabla \left(\frac{B_\phi}{r} \right) = -\frac{\partial \Omega}{\partial r} \frac{\partial (rA)}{\partial z} + \frac{\partial \Omega}{\partial z} \frac{\partial (rA)}{\partial r}, \tag{5}$$

plus the equations of conservation of mass and energy (the adiabatic equation for simplicity), where A is the z -component of the vector potential, $\mathbf{B}_p = (B_r, B_z)$ is the poloidal component of the magnetic field, and Ω is the angular velocity around the z -axis, and

$$\mathbf{g} = -\nabla\psi, \quad \psi = -GM/(r^2 + z^2)^{1/2}. \tag{6}$$

In the above, quantities are normalized by their typical value at a typical point in space in the normalized coordinate. The time is scaled by the typical length divided by the typical velocity. The set of nondimensionalized coefficients (C_1, C_2, C_3) is given by

$$C_1 \equiv v_{s0}^2/\gamma v_{\phi0}^2, \quad C_2 = V_{A0}^2/v_{\phi0}^2, \quad C_3 = v_{K0}^2/v_{\phi0}^2, \quad \text{where} \tag{7}$$

$$v_{s0}^2 = \gamma \mathcal{R} T_0, \quad V_{A0}^2 = B_0^2/4\pi\rho_0, \quad \text{and} \quad v_{K0}^2 = GM/r_0.$$

Equations (1)–(3) are the r -, z -, and ϕ -components of the equation of motion, respectively, and (4)–(5) correspond to the poloidal and toroidal components of the induction equation, respectively.

It is seen from (3) that angular-momentum loss is caused if there exists a negative gradient in B_ϕ in the direction of \mathbf{B}_p , while B_ϕ is produced if \mathbf{A} makes an angle with Ω , as seen from (5). In other words, B_ϕ is produced by being pulled around the axis by the differential rotation of the disk, and the angular momentum is lost from the disk as B_ϕ is transferred out from the disk due to the gradient in B_ϕ along \mathbf{B}_p , carried by the Poynting flux in the finite-amplitude, torsional Alfvén wave, as well as by the spinning motion of the mass in the jet. As the result, the rotation of the disk gas is braked, and the disk gas is allowed to spiral down towards the central gravitator, while the mass above the disk surface is accelerated along the direction of the axis as spinning jets.

The whole dynamical process can continue, and be amplified, with the liberated gravitational energy as the source of energy for the process.

Finite difference methods of numerical simulations are used to solve the equation system. We have used the Lax-Wendroff scheme, Roe's method, and the CIP method, with TVD modifications and others, in pursuit of improved results. We initially used the 2.5D approximation due to the restricted computational resources in the middle of the 1980s. That was intrinsically better than the 2D simulations which were beginning to be used in those days because we could take into account the essential factors, B_ϕ and v_ϕ , which are responsible for essential physics like the pinching effect and spinning motions allowing centrifugal effects, respectively. More recently, we used 3D codes in order to treat more realistic situations, e.g., the helical kink instability (Todo et al. 1993; Nakamura et al., in preparation) to pinpoint the detailed magnetic action. The magnetodynamic mechanism has also been extended by Stone & Norman (1992), Matsumoto et al. (1997), Kudoh et al. (1997), and Nakamura et al. (in preparation).

We note here that we do not take the effects of general relativity into account because we only deal with the part of the disk at a radius 10–100 times the Schwarzschild radius (3×10^{14} cm). The effect of special relativity is now being accounted for in the simulation scheme, but the results discussed here do not contain it, because the intention here is to demonstrate the applicability of the MHD mechanism of the jet acceleration from AGNs, as we advocated. The effect of general relativity has been taken into account in the model by Koide, Shibata, & Kudoh (1998) and also discussed by Shibata, Koide, & Kudoh (2000) in these Proceedings.

2.2. Application to the AGN Case

Gravitational Contraction of Intergalactic Gas Having Weak Magnetic Field and Angular Momentum In extending the treatment to the case of AGN radio jets, we consider a region (with radius R_0) in the primordial intergalactic space in which there is a tenuous gas (density ρ_0) having a large-scale, weak magnetic field (intensity B_0). If the gas in this sphere gravitationally contracts to form a spheroidal (spherical) protogalaxy with mass M_p and radius R_p , then $M_p = (4\pi/3)\rho_0 R_0^3 = (4\pi/3)\rho_p R_p^3$ and $B_p = B_0(R_0/R_p)^2$. If we take $M_p = 10^{11} M_S$, $R_p = 30$ kpc, $n_p = 10^{-1.5} \text{ cm}^{-3}$, and $B_p = 10^{-6}$ G, then it turns out that we considered the initial state with $n_0 = 10^{-6} \text{ cm}^{-3}$ and $B_0 = 10^{-9}$ G, for $R_0 = 1$ Mpc.

In the protogalaxy, we assume that most of the gas became stars in the turmoil of contraction, and, in this turmoil, a small fraction (α_{pB} , say, of 0.01) of gas was created, having very low angular momentum, with a black hole of $10^9 M_S$ formed at the center. We further assume that a fraction (α_{Bd} , say, of 0.01 again) of the black hole mass, $10^7 M_S$, remained as an accretion disk of radius 0.01 pc surrounding the central object. If all these are the cases, and the fraction $\alpha_{pB}\alpha_{Bd}$ of the magnetic flux is kept frozen-in in the accretion disk, then the magnetic field and the density of the accretion disk will be $B_{ad} \sim 10^2$ G and $n_{ad} \sim 10^{14.5} \text{ cm}^{-3}$ on the average, respectively. The estimation of the temperature depends upon various things and is difficult. We therefore assume $T_{ad} \sim 10^6$ K and use this for estimating the coefficients for the simulations.

With these crude estimates of physical parameters derived by the simple considerations of likely geometries and their changes, we can estimate $C_1 \sim 10^{-3.5}$ and $C_2 \sim 10^{-3}$ (with C_3 of the order unity for the disk accreting to the black hole). C_1 and C_2 are considerably smaller than those in the star-formation case of, say, $C_1 = 5 \times 10^{-3}$ and $C_2 = 1.5 \times 10^{-2}$, but are conceptually in the same region of parameter space. (The thermal and magnetic energies are much smaller than the gravitational energy, and the gas is basically in rotational equilibrium but *is affected* by the angular-momentum loss due to magnetic tension. It is seen later that the lower-density surface layers of the toroid lose the most angular momentum and accrete like an avalanche. Thus, the coefficients are effectively much closer.) Namely, the situation of AGN belongs conceptually to the same category as that of star formation, except that the effect of gravity is naturally more dominant in the AGN case than the star-formation case. This conceptual similarity is the explanation for the occurrence of jetting in the star-formation and AGN cases although the scales and physical parameters differ by orders of magnitudes in those objects belonging to different astronomical hierarchies. The situation in detail is, of course, not the same. For example, the temperature of the disk gas may be much higher in the AGN case; we may better use such a model for the disk like the “Abramowicz toroid”, which is in rotational equilibrium with the gas-pressure effect.

Results for the AGN Case We show some results of simulations for a jet-producing AGN (Uchida et al. 1999).

The first point in the results of simulation is that the magnetic braking effect allows the accretion of disk material towards the central gravitator. In the present case of an accretion toroid, it is clearly seen that the infalling gas comes from the surface of the toroid that loses the most angular momentum, while the denser gas deep inside the disk is less affected. Therefore, the accretion takes the form of avalanches like the surface of snow sliding down over the hills.

It is seen that the avalanches produce a tipped magnetic field configuration stretched into azimuthal as well as inward directions. There is another tip coming up from the lower surface, and magnetic reconnection can occur at the equatorial plane at the innermost part of the toroid. This may well contribute to the production of the seed high-energy electrons, and those are injected into the jets.

Physically, the braking means the transfer of angular momentum from the disk surface gas to different parts via magnetic tension, mainly the magnetized gas in the disk corona, and that is set into rotation in the same direction as the disk. This extends in time in the form of nonlinear, torsional Alfvén wave trains (TAWT). The shell here is the conical-cylindrical shell, as in Figure 1a, in which the toroidal field is provided from the innermost part of the disk.

Another point to be discussed is the relation of our mechanism of enhancement of accretion to the so-called Balbus-Hawley instability. Balbus & Hawley (1991) treated the linear version of angular-momentum transfer that we *had* treated in our model (Uchida & Shibata 1985). Our treatment of the nonlinear regime of the same effect was 2.5D and did not accommodate the perturbations in φ . Even with $k_\varphi = 0$, Balbus & Hawley’s results predict a chaotic growth of the magnetic field bending in the (r, z) -plane, but this did not occur much in our simulation. One possible explanation may be that the fastest growing

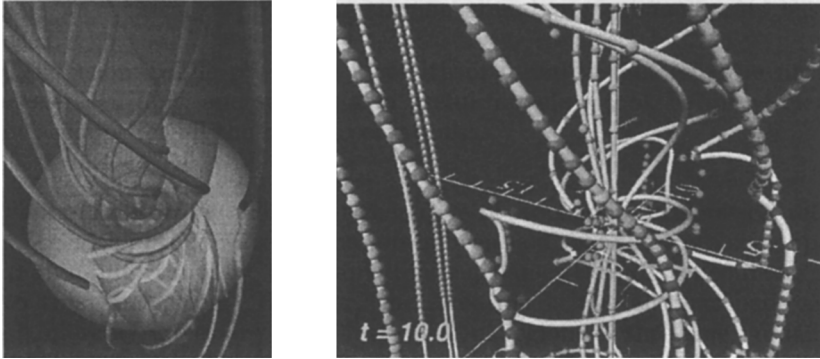


Figure 1. (a) 3D Presentation of the Behavior of the Model. Surface layers of the toroid are avalanching toward the central gravitator due to the braking effect producing twisted magnetic field lines. Note that the field lines are brought around the axis as well as toward the center with tips that eventually reconnect with the counterpart coming up from the lower surface. (b) The Behavior of Test Particles on the Magnetic Field Lines. It is seen that the field lines are carried around the axis due to the rotation of the disk material—the closer ones faster, the distant ones slower. The parts of the field lines imbedded in the gas near the surfaces “avalanches” toward the axis due to the most efficient angular-momentum loss. The pseudo-Lagrangean fluid particles are seen to be whirled up due to the centrifugal acceleration after the initial push up by the gradient of the magnetic pressure of the toroidal magnetic field. Also, the gas on the near-axis part is squeezed out as a jet pushed by the gas pressure.

mode, our global surface avalanching mode, grows dominantly first and suppresses the small and slower-growing modes by exerting an additional tension in the φ -direction. In other words, the situation exerts a “line-tying” effect by stretching the field lines and may stabilize the small-scale instability Balbus & Hawley talked about in their treatment.

We show in Figure 1 the result of dynamic simulation in a 3D presentation. The tipped configuration of the magnetic field that will make reconnections is seen together with the much smaller effect, related to what Balbus & Hawley talked about, pushing the gas in the equatorial part of the disk outward also by the angular-momentum transfer to that part, though the effect is much smaller since the density inside the disk is much higher.

2.3. Discussion of Some Other Phenomena Inherent to the Model

For example, this model explains most naturally the helical magnetic field inside the jets, as well as the structural helix due to the helical kink instability in the

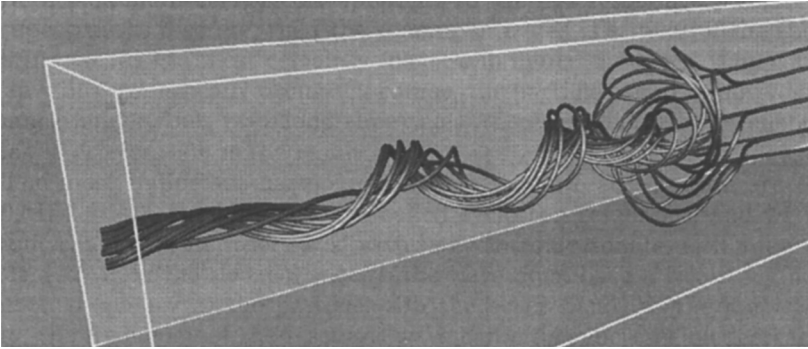


Figure 2. 3D MHD simulation of the formation of helical structure due to the helical kink instability when the TAWT encounters the border of the “cavity”. This explains the structural wiggles of the observed jets (Nakamura *et al.*, in preparation).

region in which the toroidal component exceeds the Kraschal-Shafranov limit. This is expected when the TAWT encounters a higher density part. One possible case will be when the TAWT encounters a high-density region along the jet path (Todo *et al.* 1993). Another and more fundamental case will occur when the front of the TAWT impinges on the outer boundary of the “cavity” (Figure 2) from which the gas contracted to the central condensation. The Alfvén velocity drops at the border, and the toroidal component accumulates to allow stronger pinching (corresponding to the hotspot). Furthermore, the bounced TAWT causes a strong toroidal field region. A helical kink instability will grow and produce a wiggled structure in which the structural wiggle and the direction of the projected magnetic field and the line-of-sight components may well be in the relation of “threads and a wiggled rope”.

The radio lobes in our model may be explained by the tucked-up, large-scale, hourglass-shaped magnetic field and the progressing pinch along the axis (Figure 2, Nakamura *et al.*, in preparation). The hourglass-shaped field is progressively made into slender jets by the sweeping pinch. The hotspots, actually the location of the intense synchrotron emission, may be produced at the “hub” of that tucked-up, initially hourglass-shaped magnetic structure at the end of the axis (jet).

We may be able to explain the acceleration and re-acceleration of electrons that are necessary in explaining the radio observations of jets and lobes, together with hotspots, in the following way. The seed electrons are considered to be accelerated in magnetic reconnections when the tips of the avalanches meet at the innermost part of the toroid. Those accelerated seed particles are released onto open field lines (sent into the large-scale jets), together with the mass of the jet ejected from the innermost part of the disk, and will be re-accelerated by the sweeping pinch.

We note that when the TAWT comes out to the very low density part in the “cavity”, the TAWT becomes a very large amplitude, circularly polarized electromagnetic wave. This may be a different mode version of the very large amplitude electromagnetic wave emitted from a pulsar in the magnetic-dipole radiation mode, and may be quite effective in accelerating particles.

As the high-energy particles travel along the jet, they lose energy to synchrotron emission; there should be a mechanism for re-accelerating these particles. Our proposal for this is as follows. The passage of the pinching fronts (very large amplitude electromagnetic waves) are felt by the particles previously accelerated; then, those particles will be re-accelerated by repeated “surfing” due to such successive passages of sweeping pinches. This is most effective when the particles begin to be trapped between the foregoing sweeping pinch front and the following front because the foregoing front is decelerated especially near the border of the cavity (returning to an Alfvén wave), and when the Fermi I acceleration mechanism begins to operate between the mutually approaching fronts. Those accelerated particles will be eventually dumped into the highly pinched magnetic field at the end point of the jet, and this may explain the hotspots with enhanced synchrotron emission.

3. Discussion

In our model, we have assumed the presence of a weak, large-scale magnetic field in the primordial intergalactic space. The 10^{-9} G magnetic field is talked about in other contexts, but it is true that there is no direct, observational evidence for this yet. Therefore, it should be mentioned that there is another possibility that the magnetic field is pulled out *from* the central body. The reason we did not choose this possibility is that without the large-scale longitudinal field, the continued production of the toroidal field will result in a very strong, helical instability that starts right outside the disk and will never produce a slender jet. In our sweeping pinch process, the longitudinal field, though weak initially, is pinched and achieves a considerable strength to oppose the pinching by the toroidal field to maintain the shape of a jet, though allowing as much as a wiggle.

But it may still be asked whether there actually exists a large-scale magnetic field in the case of an AGN environment, although the existence and the role of the magnetic field are supported in the star-formation case. This is a crucial point for our model, and observational establishment of the presence of a large-scale magnetic field is required. An argument for the presence of the large-scale magnetic field in intergalactic space might be that the AGN’s radio jets were formed on the border of cosmic voids into which the very weak, cosmic magnetic field may have been swept up (Biermann 2000) and become appreciable, of the order of 10^{-9} G. If that is the case, there might be some correlation between the direction of the radio jets and the borders of the voids—either a higher probability for the jets to be parallel to, or a higher probability of finding BL Lac objects on, the borders of cosmic voids (much farther than the optically confirmed voids), although the directions of the jets on the front and back sides of the borders of the cosmic voids can be seen less systematically.

It is stressed here that the presence of the characteristic magnetic feature indicating a helical field in the jets and tails remote from the AGN core *will*

give pretty firm support for the idea that a magnetodynamic mechanism is responsible for the acceleration and collimation process *at the center*. Since such a systematic field carrying a considerable amount of energy can not be produced by processes in the vicinity of the remote parts of a jet, we can say that what is producing the jets and tails (as well as the lobes with hotspots at their tips) is the magnetodynamic effect sent out from the powerful central engine—the magnetized accretion disk—in the form of systematic large-amplitude, torsional Alfvén waves. The recently found, very large, Lorentz-factor phenomena may well be byproducts, and the magnetodynamic effects should be able to come out without being hindered.

References

- Balbus, S. A., & Hawley, J. F. 1991, *ApJ*, 376, 214
Blandford, R. D., & Payne, D. G. 1982, *MNRAS*, 199, 883
Biermann, P. 2000, *Ap&SS*, in press
Eilek, J., & Owen, F. 2000, *ApJ*, submitted
Feretti, L., Perley, R., Giovanni, G., & Andernach, H. 1999, *A&A*, 341, 29
Koide, S., Shibata, K., & Kudoh, T. 1998, *ApJ*, 495, L63
Kudoh, T., & Shibata, K. 1997, *ApJ*, 476, 632
Matsumoto, R., Uchida, Y., Hirose, S., Shibata, K., Hayashi, M., Ferrari, A., Bodo, G., & Norman, C. 1997, *ApJ*, 461, 115
Nakamura, M., Uchida, Y., & Hirose, S., in preparation
Owen, F., Hardee, P., & Cornwell, T. 1989, *ApJ*, 340, 698
Perley, R., Bridle, A., & Willis, A. 1984, *ApJS*, 54, 291
Perlman, E., Biretta, J., Zhou, F., Sparks, W., & Macchetto, F. 1999, *AJ*, 117, 2185
Pudritz, R. E., & Norman, C. A. 1986, *ApJ*, 301, 571
Shibata, K., Koide, S., & Kudoh, T. 2000, these Proceedings
Shibata, K., & Uchida, Y. 1986, *PASJ*, 38, 631
Stone, J. M., & Norman, M. L. 1992, *ApJS*, 80, 791
Todo, Y., Uchida, Y., Sato, T., & Rosner, R. 1993, *ApJ*, 403, 164
Uchida, Y. 2000, Panel Discussion Session in these Proceedings
Uchida, Y., Nakamura, M., Hirose, S., & Uemura, S. 1999, *Ap&SS*, 264, 195
Uchida, Y., & Shibata, K. 1985, *PASJ*, 37, 515
Uchida, Y., & Shibata, K. 1986, *Can. J. Phys.*, 64, 507